A three-dimensional PSME model for rotating flows in an annular cavity

A Three-dimensional PSME Model for Rotating Flows in an Annular Cavity

Ming-Jyh Chern[1,2], Nima Vaziri[1,3,*], Alistair G.L. Borthwick[4]

[1] Department of Mechanical Engineering, National Taiwan University of Science and Technology, 43 Sec. 4 Keelung Road, Taipei 10607, Taiwan

[2] Ecological Engineering Research Unit, National Taiwan University, No. 1 Sec. 4 Roosevelt Road, Taipei 10617, Taiwan

[3] Department of Physics, Karaj Branch, Islamic Azad University, Karaj, Iran

[4]Department of Civil and Environmental Engineering, University Collage Cork, Cork, Ireland

[*] E-mail: n.vaziri@gmail.com; Tel: (886)-2-2737-7315; Fax: (886)-2-2737-6460

Abstract

A pseudospectral matrix-element (PSME) numerical model is described for the simulation of rotating flows in a three-dimensional annular cavity. Temporal discretization is implemented using a second-order semi-implicit scheme. Modified compressibility is invoked to handle the coupling between velocity and pressure while maintaining the incompressibility constraint. The governingcontinuity and Navier-Stokes momentum equations and boundary conditions are discretized using Chebyshev and Fourier collocation formulae. The model is validated against numerical results from alternative schemes and experimental data on rotating flows in an annular cavity. A base flow regime and instability patterns are observed, in accordance with other previously

published investigations. It is demonstrated that the PSME model provides an accurate representation of rotating flows in an annular cavity.

Keywords: PSME method; Rotor-stator cavity.

1. Introduction

Confined cavity flow between a pair of coaxial discs is relevant to many industrial devices involving rotating fluids, such as turbomachinery. In many cases, such flows can be assumed to be incompressible and Newtonian in behaviour, and so can be described by mass continuity and the Navier-Stokes momentum equations. It is well known that very few exact solutions can be obtained for the Navier-Stokes equations owing to their non-linearity. One such family of solutions exists however for stationary axisymmetric laminar flow. Historically, von Kármán's (1921) study about a laminar flow over an infinite rotating disc in a quiescent fluid can be taken as a useful starting point. This flow is nowadays known as generalized von Kármán swirling flow. Later, Bödewadt (1940) carried out an important numerical investigation into the flow over an infinite stationary plane with an outer flow in solid body rotation. Batchelor (1951) considered stationary axisymmetric flow between two discs of infinite radii, and argued that boundary layers would develop on both discs in the case of a single rotating disc. Meanwhile Stewartson (1953) found that only one boundary layer developed, near the rotating disc. Over the past half century, Batchelor and Stewartson flows have been investigated by many researchers, including Lance and Rogers (1962) and Zandbergen and Dijkstra (1987) who

showed that the such flows which progressively appear as the Reynolds number increases are merely two of several solutions to the governing viscous flow equations.

Numerous theoretical (e.g. Faller, 1991 and San'kov and Smironov, 1992), experimental (e.g. Moisy *et al.*, 2004, Schouveiler *et al.*, 2001 and Gauthier *et al.*, 1999) and numerical (e.g. Serre *et al.*, 2001, Nore *et al.*, 2003 and Poncet *et al.*, 2009) studies have been undertaken into rotating flows between discs. The majority of these studies were concerned with the stability of the flow. Owen and Rogers (1989) discussed the engineering applications of rotating annular flows. Recently, Launder *et al.* (2010) carried out a comprehensive review of literature concerned with flow in rotor-stator cavities. [AND WHAT DID LAUNDER *ET AL.* CONCLUDE ???].

Spectral methods are highly accurate numerical techniques that are appropriate for solving certain problems in fluid mechanics (see e.g. the detailed review by Hussaini and Zang, 1987). Recently, Boyd and Yu (2011) compared seven spectral methods used to solve the Poisson equation in a disc. The present study employs the pseudospectral matrix-element (PSME) method of Ku and Hatziavramidis (1985) to solve the three-dimensional continuity and Navier-Stokes equations for incompressible viscous flow in a rotating annular cavity. Due to its spectral accuracy (Canuto *et al.*, 1988), the PSME method is well suited to solving boundary value partial differential equations. Moreover, the PSME method solves the governing equations in physical space instead of a spectral domain, and so is computationally more efficient than conventional spectral methods.

The PSME approach has also been successfully applied to a variety of free surface problems (see e.g. Chern *et al.*, 2005, 2011 and Vaziri *et al.*, 2011).

A cylindrical coordinate system is chosen to model the annular cavity. The governing Navier-Stokes equations are temporally discretized using a combination of Adams-Bashforth (AB) and Crank-Nicolson (CN) methods for the advection and the diffusion terms, respectively. The proposed discretization uses a Fourier pseudospectral matrix (FPSM) in the angular direction and a Chebyshev pseudospectral matrix (CPSM) in the radial and the axial directions. Due to the CN method, the discretized Navier-Stokes equations are partially implicit, leading to an asymmetrical set of equations, which are solved using the bi-conjugate gradient method. To avoid singular behavior when the radial coordinate tends to zero, an inner cylinder of arbitrary radius is inserted along the centerline axis of the cylindrical domain. It should be noted that numerical difficulties related to the velocity-pressure coupling are overcome using the modified compressibility approach (Chorin, 1968).

2. Mathematical model and physical parameters

Figure 1 illustrates the annular cavity. The geometry comprises a pair of smooth coaxial parallel discs that enclose an annular domain of internal wall radius a and external wall radius b, respectively. The upper (stator) disc of the cavity is stationary and the lower (rotor) disc rotates at uniform angular velocity Ω. The lateral boundaries of the flow domain are composed of two cylinders each of height h. The inner and the outer cylinders are the so-called hub and shroud, respectively.

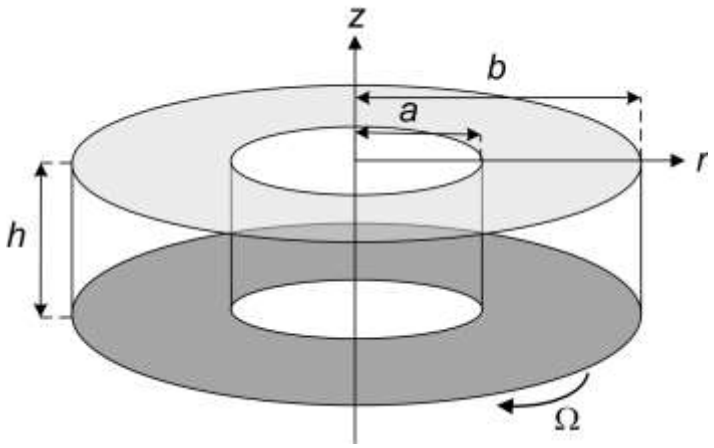

Figure 1. Schematic view of the annular rotor-stator cavity.

The flow is controlled by three main parameters: the Reynolds number *Re*, the aspect ratio, and a curvature parameter. The Reynolds number is usually based either on the outer radius of the cavity, $Re = \Omega b^2 / \nu$ (e.g. Owen and Rogers, 1989, Schouveiler *et al.*, 1999 and Poncet *et al.*, 2009) where ν is the fluid kinematic viscosity or on the height of the cavity, $Re = \Omega h^2 / \nu$ (e.g. Sirivat, 1991, Gauthier *et al.*, 1999 and Serre *et al.*, 2001). The latter is chosen in the present study because it scales the characteristic boundary layer thickness, $\delta = (\nu / \Omega)^{1/2}$, with respect to the cavity height. The aspect ratio is defined as $G = h / b$ and the curvature parameter is $R_m = (b + a) / (b - a)$.

3. Numerical method

3.1. Governing equations

In this problem, 3D unsteady incompressible viscous fluid flow without energy transfer is considered. The governing continuity and Navier-Stokes momentum equations can be written

$$\nabla \cdot \mathbf{u} = 0, \qquad (1)$$

and

$$\frac{\partial \mathbf{u}}{\partial t} + (\mathbf{u} \cdot \nabla)\mathbf{u} = -\frac{1}{\rho}\nabla p + \nu \nabla^2 \mathbf{u}, \tag{2}$$

where **u** is the velocity vector, t is the time, ρ is the fluid density, p is pressure, and v is the kinematic viscosity. Along the cylindrical coordinate directions (θ, r, z), the velocity components are $\boldsymbol{u}_\theta$, $\boldsymbol{u}_r$ and $\boldsymbol{u}_z$, respectively. All above parameters are used in nondimensional forms. [GIVE DETAILS ON HOW THE PARAMETERS ARE NON-DIMENSIONALISED]

3.2. Modified compressibility method

Because of the absence of pressure in the continuity equation, a special scheme must be implemented in order to evaluate the pressure. The present study makes use of a two-step modified compressibility method (Cortes and Miller, 1994) to calculate the pressure. In the first step, the continuity equation is modified to

$$\frac{p^*}{\lambda} + \nabla \cdot \mathbf{u} = 0, \tag{3}$$

where λ is a prescribed small number and p^* is the calculated pressure correction term. In the second step, the pressure field is corrected as follows,

$$p^{new} = p^{old} + p^*. \tag{4}$$

The continuity equation is satisfied when $p^* \to 0$. The two-stage technique is applied iteratively each time step until the absolute value of the first term in Equation (3) is less than the prescribed tolerance (see Chern *et al.*, 2005 for more details).

3.3. Temporal discretization scheme

Herein, Crank-Nicolson (CN) and second-order Adams-Bashforth (AB) schemes are used to integrate the diffusion and advection terms forward in time. The discretized Navier-Stokes equation becomes

$$\frac{\mathbf{u}^{n+1}-\mathbf{u}^{n}}{\Delta t}+\frac{3}{2}(\mathbf{u}^{n}\cdot\nabla)\mathbf{u}^{n}-\frac{1}{2}(\mathbf{u}^{n-1}\cdot\nabla)\mathbf{u}^{n-1}=-\nabla p+\frac{1}{Re}(\frac{1}{2}\nabla^{2}\mathbf{u}^{n+1}+\frac{1}{2}\nabla^{2}\mathbf{u}^{n}). \tag{5}$$

The CN method is a second-order partially implicit scheme whereas the AB method is fully explicit. Therefore, the mixed AB-CN approach is second-order semi-implicit. This combination has good stability properties.

3.4. Pseudospectral model

Like other spectral methods, the pseudospectral matrix-element (PSME) method is based on orthogonal polynomials. Herein, Chebyshev polynomials are used for derivative expansions in the radial and the vertical directions and Fourier polynomials are used in the angular direction. This scheme is based on that of Chern *et al.* (2001, 2005). The domain is discretised according to the Chebyshev and Fourier collocation grid formulae as follows:

$$\theta_i=\frac{2i\pi}{N},\ r_j=\cos\left(\frac{j\pi}{M}\right),\ z_k=\cos\left(\frac{k\pi}{L}\right), \tag{6}$$

for $i = 0, 1, \ldots, N\text{-}1, j = 0, 1, \ldots, M,$ and $k = 0, 1, \ldots, L$, where N, M and L are the number of collocation points in the θ, r and z directions, respectively. Figure 2 depicts an example of the physical grid system. Chebyshev collocation points are separately distributed in the central part of the interval [-1, 1] but concentrated at the two ends of the domain. Fourier collocation points are uniformly located within $[0, 2\pi]$.

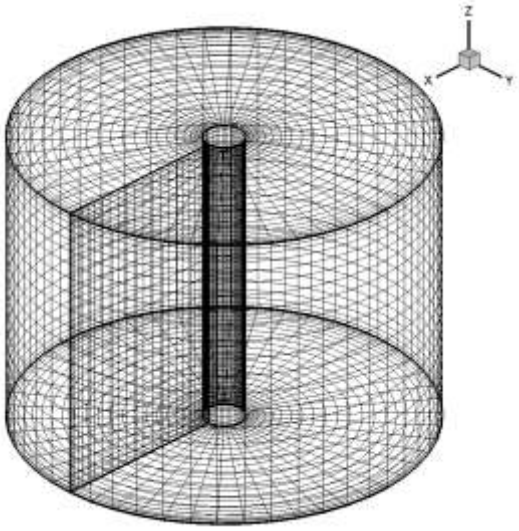

Figure 2. The three-dimensional pseudospectral mesh.

Using equation (6), the collocation grid system is created in the physical domain. Now, the Fourier pseudospectral matrix (FPSM) and Chebyshev pseudospectral matrix (CPSM) are established as follows. Consider a continuous function $\varphi(x)$. The qth derivative at each collocation point (x_j) is approximated by

$$\frac{\mathrm{d}^q \varphi}{\mathrm{d}x^q} = \sum_{k=0}^{N} \hat{G}_{j,k}^{(q)} \varphi_k , \tag{7}$$

where $\hat{\mathbf{G}}^{(\mathbf{q})}$ is the CPSM for the qth derivative. Moreover, for the same scheme, the qth derivative at the Fourier collocation point x_j is given by

$$\frac{\mathrm{d}^q \varphi}{\mathrm{d}x^q} = \sum_{k=0}^{N-1} \hat{F}_{j,k}^{(q)} \varphi_k , \tag{8}$$

where $\hat{\mathbf{F}}^{(\mathbf{q})}$ is the FPSM for the qth derivatives. More details about the PSME method are given by Ku *et al.* (1987) and Chern *et al.* (2011).

3.5. Boundary conditions

Non-slip boundary conditions ($\boldsymbol{u}_\theta = \boldsymbol{u}_r = \boldsymbol{u}_z = 0$) are applied at all rigid walls. On the rotating disc, the angular component of velocity is set to $\Omega\,(1+r)\,/\,2$ while the other velocity components are fixed at zero. Physically, there is a thin gap between the edges of the rotating disc and stationary sidewalls. This junction layer involves a singularity in angular velocity. To eliminate this problem, the boundary condition is smoothed using an exponential angular velocity profile $\boldsymbol{u}_\theta = \exp((z-1)/0.006)$ following Maubert *et al.* (1993) and Serre *et al.* (2004).

3.6. Matrix solver

The discretised Navier-Stokes equations are semi-implicit, and so a set of non-symmetrical simultaneous equations are formed. Herein, the bi-conjugate gradient method (Jennings and McKeown, 1992) is selected as the solver. In addition, the storage method described by Press *et al.* (1986) is used to hold the non-zero elements of the sparse matrix.

4. Results and discussion

The model is now used to simulate rotating flow in the cavity. The general behavior of the flow is analyzed in detail and compared with results from other investigations. First, base flow is considered in order to verify the model. Next, mesh convergence and time step dependency are assessed. Finally, a parameter study is undertaken, and several

instability patterns investigated. The main parameters are limited to $G = [0.05, 2.0]$, $R_m = [1.1, 3.5]$, and $Re = [1200, 140000]$, covering a wide range of annular flow behaviour.

4.1. Base flow

Laminar base flow between a pair of rotating discs is steady, axisymmetric and three-dimensional. As already mentioned, the two best-known theoretical general solutions of this flow are those of by Batchelor (1951) and Stewartson (1953). The two global parameters of the flow in the cavity are linked together by the relation $Re_b = ReG^2$. For large Re_b, the base flow in a closed geometry is similar to the Batchelor solution. The rotor boundary layer is an Ekman layer. Flow in this layer is directed outward because the radial velocity component is positive. Meanwhile, the boundary layer in the vicinity of the stator is the so-called Bödewadt layer. The flow in this layer is directed inward and the radial velocity component is negative. Figure 3 shows an example of the base flow for $R_m = 1.1$, $G = 0.2$, and $Re = 1200$ (such that $Re_b = 48$). The radial recirculating flow pattern is in close agreement with the received understanding from previous studies (see e.g. Serre *et. al.*, 2001).

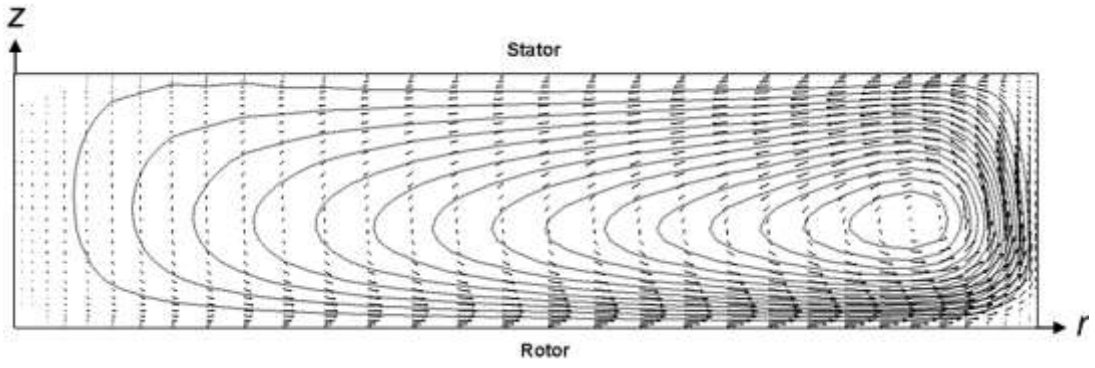

Figure 3. Velocity vectors and stream function contours in the plane $(0, r, z)$; $R_m = 1.1$, $G = 0.2$, $Re = 1200$.

The thickness of the boundary layer is usually normalized by its characteristic length, $\delta = (\nu / \Omega)^{1/2}$. Figure 4 depicts the normalized thicknesses of the Ekman and the Bödewadt boundary layers as functions of non-dimensional radial distance r for $R_m = 1.1$, $G = 0.2$, $Re = 1400$. The present results are similar to those of Serre *et al.* (2001) and match the experimental results of Gauthier *et al.* (1999) [THESE SHOULD ALSO BE PLOTTED ON FIGURE 4]. It can be seen that the Ekman layer remains constant whereas the Bödewadt layer thickness decreases from the hub to the shroud. Near the vertical walls, the layers become almost merged and cannot be measured accurately.

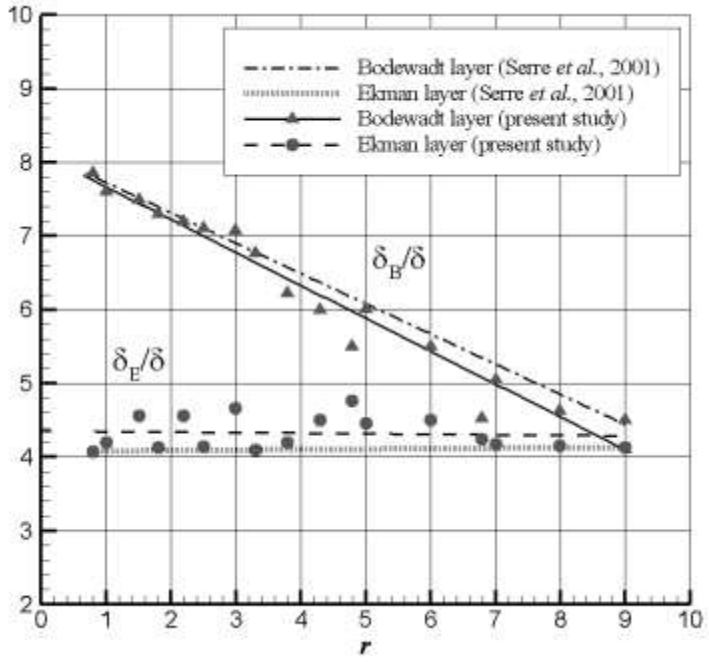

Figure 4. Development of normalized thickness of boundary layers as a function of non-dimensional radial distance (data are fitted linearly): $R_m = 1.1$, $G = 0.2$, $Re = 1400$.

The boundary layer thicknesses are influenced by the values of G and Re. Figure 5 compares the axial profile of the radial velocity component u_r for aspect ratios of 0.2, 0.5 and 2.0. In all cases, the Reynolds number is 70,000 and the curvature parameter is 3.5. As would be expected, when $G = 0.2$, the boundary layers become joined together, and so are thicker than other cases. An inviscid region is created as the aspect ratio increases. In the tallest cavity, the stator boundary layer has almost vanished and the flow is like a typical Stewartson flow.

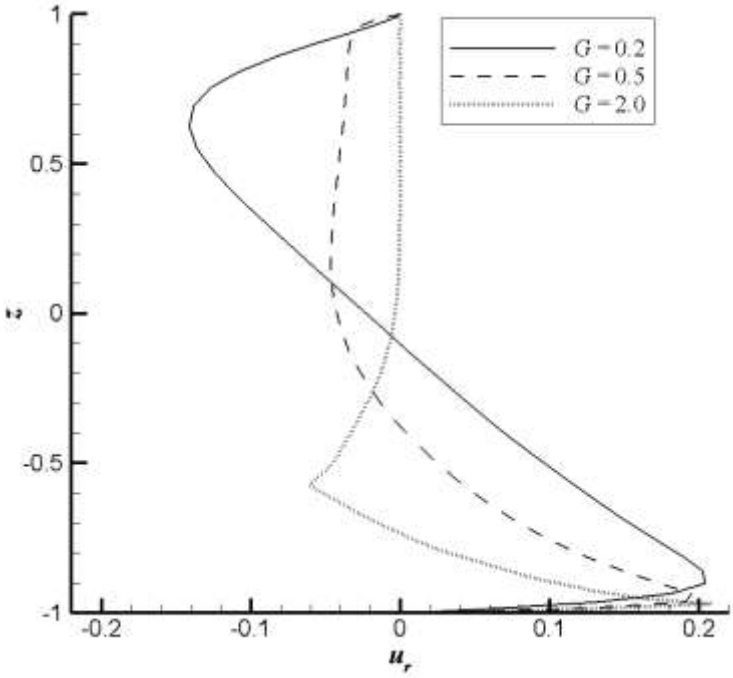

Figure 5. Axial profile of the radial velocity component at the mid-radial location for $R_m = 3.5$, $Re = 70000$, and $G = 0.2$, 0.5 and 2.0.

Figure 6 shows the axial profile of the mean velocity in the annular cavity for $R_m = 1.1$, $G = 0.05$, and $Re = 36900$. The results are in satisfactory agreement with the experimental measurements obtained by Schouveiler *et al.* (2001). It should be noted

that the non-viscous part of the flow in the center of the cylinder does not develop fully because the axial component of velocity is not strictly zero. Also, Schouveiler *et al.*'s (2001) measurements are limited in the boundary layers. Similar results were also reported by Dijkstra and van Heijset (1983).

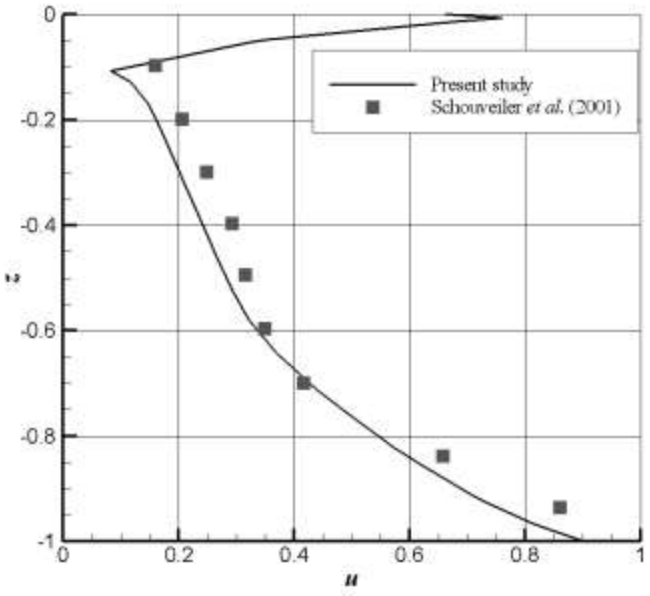

Figure 6. Axial profile of normalized mean velocity for $r/b = 0.357$, $R_m = 1.1$, $G = 0.05$, and $Re = 36900$.

The ratio between convective and Coriolis motions defines an entrainment coefficient (or local Rossby number) $K = \Omega_f / \Omega$ where Ω_f is the local angular velocity of the fluid. For an infinite-disc cavity, laminar similarity solutions give a constant value, $K = 0.313$ (Pearson, 1965 and Itoh, 1991). For a finite-disc cavity, both experimental (e.g. Gauthier *et al.*, 1999) and numerical (e.g. Serre *et al.*, 2001) results show that K is an increasing function of the radius. As found in other studies, the entrainment coefficient increases monotonically with radius, and so the core fluid rotation rate increases from the

hub to the shroud. Table 1 compares the entrainment coefficients obtained by the present study with those determined experimentally by Schouveiler *et al.* (2001) for $G = 0.05$ and $Re = 36900$ at mid-height of the cavity. A major discrepancy is evident between the predicted and measured entrainment coefficients near the hub. This may be because of the inner cylinder wall effect in the present model. However, the present results are of the same order as those of Dijkstra and van Heijst (1983) and Gauthier *et al.* (1999). It should be noted that other authors have found discrepancies between numerical predictions and experimental estimates of K. For example Serre *et al.* (2001) report a 70% overestimate. Figure 7 depicts the mean velocity contours in the plane $(0, r, z)$ and at the mid-height of the cavity.

Table 1 Local Rossby number (with r/b normalized to [0, 1])

r/b	***K* (present study)**	***K* (Schouveiler *et al.*, 2001)**
0.357	0.16	0.35
0.643	0.32	0.40
0.850	0.46	0.46

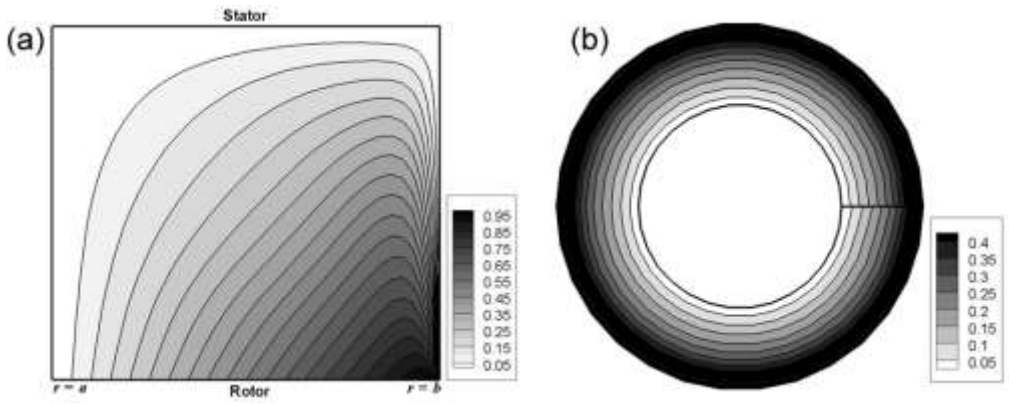

Figure 7. Mean velocity contours after 100 nondimensional time units (a) in the plane of (0, r, z), (b) at the mid-height of the cavity: $R_m = 3.5$, $G = 0.2$, $Re = 4000$.

4.2. Spectral and temporal resolutions

Previous studies have shown that the PSME method gives convergent and stable results for wide ranges of collocation point numbers and time step (see e.g. Chern *et al.*, 2011). Table 2 lists the parameters used to test for mesh convergence (number of collocation points) and numerical stability (time step). In these cases, $R_m = 1.2$, $G = 0.16$, and $Re = 26000$. Table 3 reports the results of these tests while also listing the computer time requirements. In all cases, the value of λ is set to 0.01, and the simulation run until a non-dimensional time of 50 is reached. The simulations are performed on a workstation with two Intel Xeon 3.10 GHz CPUs and 6 GB RAM.

Table 2 Mesh convergence and time step parameter study

Case	***N***	***M***	***L***	**Total no. of grid cells**	Δt^*
c1	25	20	25	13650	0.0001

c2	35	30	35	37800	0.0001
c3	35	30	35	37800	0.0005
c4	40	35	35	51840	0.0001

Table 3 Mesh convergence and time step test results (coordinates are normalized)

Case	***u*** **(0, 0.5, 0.5)**	***u*** **(0, 0.5, 0.05)**	***u*** **(0, 0.5, 0.95)**	δ_F/δ **(*r* = 0.5)**	δ_B/δ **(*r* = 0.5)**	**CPU time (*s*)**
c1	0.222	0.503	0.025	7.095	12.323	350
c2	0.253	0.500	0.013	6.445	13.727	1160
c3	0.237	0.500	0.012	6.404	10.818	2400
c4	0.246	0.523	0.012	6.404	13.161	2140

It may be observed from Table 3 that the predicted mean velocities are insensitive to the number of grid collocation points, except for Case c1. Substantial discrepancies occur in the non-dimensional boundary layer thicknesses which are not predicted to high accuracy. The maximum difference in mean velocity in Cases c2 to c4 is about 7%. Cases c3 and c4 are more expensive to compute than Case c2 in terms of CPU time. Based on these results, a collocated mesh of $35\times30\times35$ nodes and a non-dimensional time step of 10^{-4} are selected for all the remaining cases. Note that the aim of the present study is purely to test the capability of the PSME model in simulating different cases of flow in a rotor-stator annular cavity. A higher resolution mesh system is recommended for more comprehensive case studies, in particular when investigating instability at high Reynolds number.

4.3. Instabilities

Two kinds of axisymmetric instabilities arise from the steady base flow, which are referred to as Type I and Type II instabilities. Based on the linear theory of Ekman flow (Lilly, 1966), Type I is an inviscid instability due to the presence of unstable inflection points in the boundary layer velocity profiles. Type II instability is more specific to the rotating disc boundary layer. It is viscous and associated with Coriolis acceleration.

Five cases are considered involving instability. Table 4 lists the parameters. Cases c2 to c4 examine the effect of Reynolds number for a fixed value of the curvature parameter, whereas Cases c1, c2 and c5 examine the influence of the curvature parameter at constant *Re*. In all cases, Type II instabilities arise which have characteristic circular ring patterns. Figure 8 shows the axial velocity component iso-surfaces for Cases c1 to c4. For Case c1, the solution becomes oscillatory, but this is not typical behavior (see Serre *et al.,* 2004 for further details). The primary destabilization occurs in the stator boundary layer at a local radius related to the critical local Reynolds number, $Re_c = (\Omega_f r_c^2 / \nu)^{1/2}$, where r_c is the critical radial location at which the pattern appears. In Case c1, the waves persist to the hub because the inner radius is larger than r_c. The radial wavelength is defined as $\lambda_r = \Delta r / n_r$, where Δr is the radial length occupied by the n_r rolls. For example, in Case c1, $\lambda_r / \delta = 11$ which agrees with the result obtained by Savas (1987) for $G = 0.5$ and $Re = 38528$. The temporal frequency $\sigma = 2\pi f$ is about 5, which is also the same as found by Savas and close to that of Gauthier *et al.* (1999) ($\sigma = 4$) for $G = 0.047$ and $Re = 110$. In Case c2, the boundary layers are merged and Type II

instabilities appear as circular rings above the lower threshold at $Re_c = 62$. This is in agreement with the findings of Serre *et al.* (2001). The upper threshold value of Re_c is about 160.

Table 4 Cases for instability parameter study

Case	***G***	***Re***	R_m
c1	0.5	25000	3.5
c2	0.2	25000	1.1
c3	0.2	70000	1.1
c4	0.2	140000	1.1
c5	0.5	25000	2.0

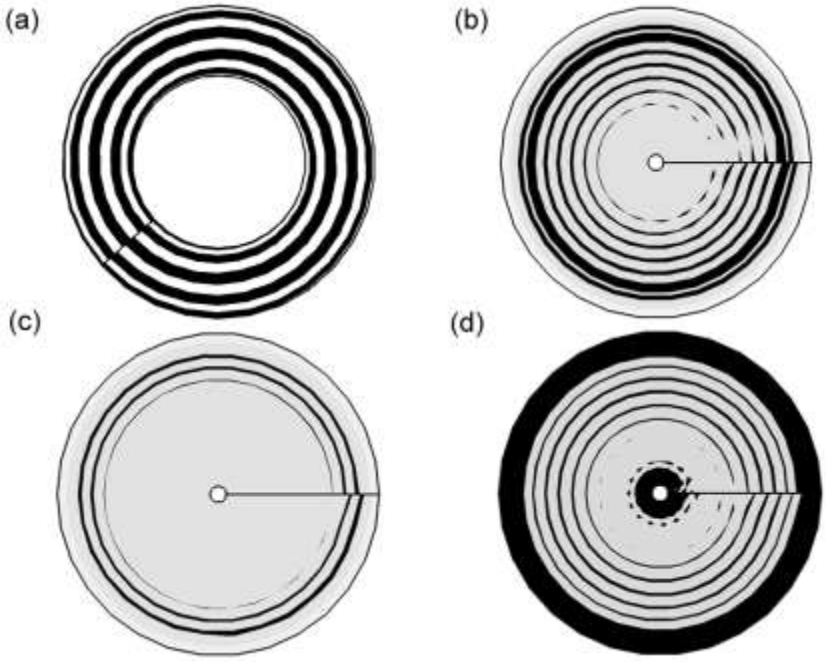

Figure 8. Iso-surfaces of the axial velocity component; Cases: (a) c1, (b) c2, (c) c3, and (d) c4.

Figure 9 shows the time evolution of the three velocity components for Case c1 (after an initial start-up period of 100 non-dimensional time units) at the mid-height of the cavity, (0, 0.5, 0.5). Figure 10 shows the corresponding power spectrum, which contains several interesting features. The largest values of power spectral density are obtained consistently with angular frequency at the mid-height of the cavity. The peak value of the power spectrum obtained at mid-height occurs at a frequency of 0.9013 rad/s that corresponds to the fundamental frequency of oscillation of the local angular velocity component. Near the rotor, a wide range of different frequencies is excited (contrary to the Bödewadt boundary layer). Along with an initial maximum at a very low frequency of about 0.5 rad/s, a distinct series of spectral peaks occurs near the rotor at integer multiples of 7 rad/s, from 7 rad/s to 35 rad/s inclusive, followed by a major peak at 40.11 rad/s (also evident at mid-height). The oscillation starts in the stator boundary layer and propagates to the rotor. The largest velocity amplitude is observed near the stator (especially near vertical walls) and it is gradually decreased to the rotor. [WHERE IS THIS EVIDENT IN FIGS 9 OR 10 ???]

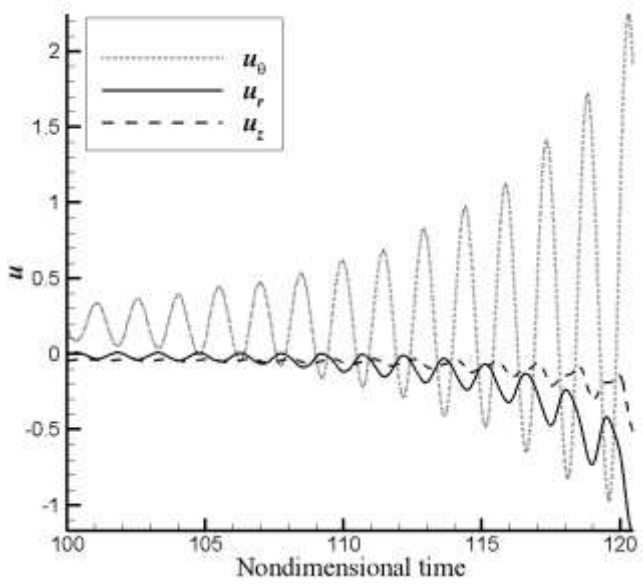

Figure 9. Time histories of velocity components at point (0, 0.5, 0.5); R_m = 3.5, G = 0.5, Re = 25000.

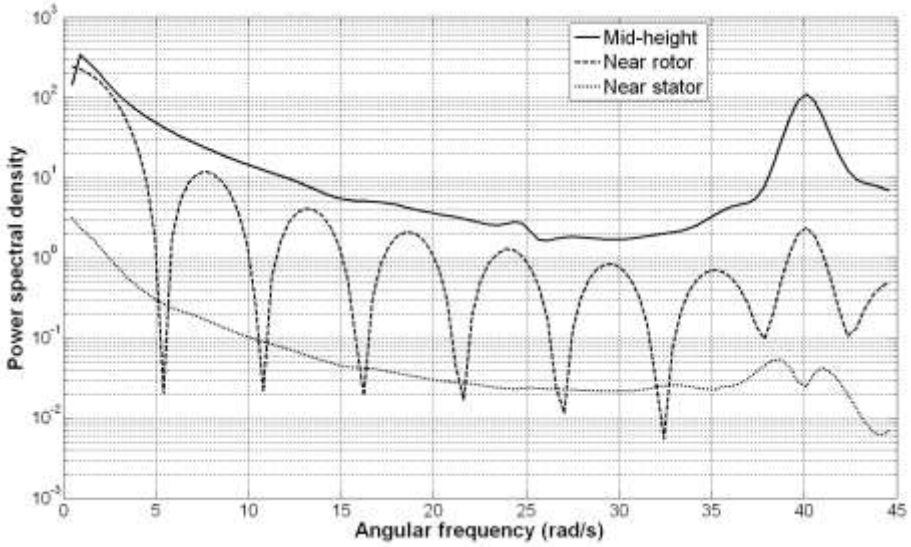

Figure 10. Power spectrum densities at different axial locations (in logarithmic scale): R_m = 3.5, G = 0.5, Re = 25000.

Rolls which progress as axisymmetric rings can break and form spirals travelling within the cavity. This spiral mode is the so-called Type I instability. In numerical studies, the spiral patterns are usually obtained by superimposition of infinitesimal disturbances to break down the rolls (contrary to experimental findings). Several studies have shown that this mode also can be created without any perturbations for certain configurations (see e.g. Poncet *et al.*, 2009). Here we do not use any perturbations. Figure 11 depicts the iso-surfaces of the axial velocity component in the stator boundary layer for Cases c3 and c5. In the other cases considered, spirals were not obtained before the end of the simulation period of 150 non-dimensional time units. In accordance with the findings of Schouveiler *et al.* (2001), spiral structures are first created near the stator and gradually propagate to the rotor but with reduced magnitude. Moreover, some of the rolls become disrupted, especially near the shroud.

At the lowest rotation rate threshold [???], the spiral wave pattern can co-exist with the previous circular waves (Savas, 1987). This phenomenon can be seen in Case c5. Previous studies (see e.g. Serre and Pulicani, 2001) have reported the co-existence of rolls and spirals during transition periods between the two types of instability. In addition, it is usually found that spirals are created near the shroud and then propagate inward. Case c5 is qualitatively similar to a case considered by Moisy *et al.* (2004) who found that a spiral structure developed near the hub. The spirals invariably have a negative orientation. In the present study, the radial wave length of the spirals is about 27δ, with twelve spiral arms formed at an angle to the azimuthal direction of about 24° near the stator. Both the radial wave length and the angle to the azimuthal direction are

in agreement with results obtained by Serre and Pulicani (2001) and Gauthier *et al.* (1999).

In Case c3, both types of instabilities are observed (see Figures 8 (c) and 11 (a)). Here, the spiral has 14 arms with a tangential angle of about 25°. It should be noted that Poncet *et al.* (2009) obtain 19 spiral arms at a tangential angle of 24° for $Re = 41000$. In Case c4 where $Re = 140000$, the spirals disappear and the Type II instability persists until the end of simulation, although some perturbations are created near the hub as can be seen in Figure 8 (d). In their experimental study of rotating flows in an annular cavity, Schouveiler *et al.* (2001) also observed the disappearance of spirals at relatively high Re.

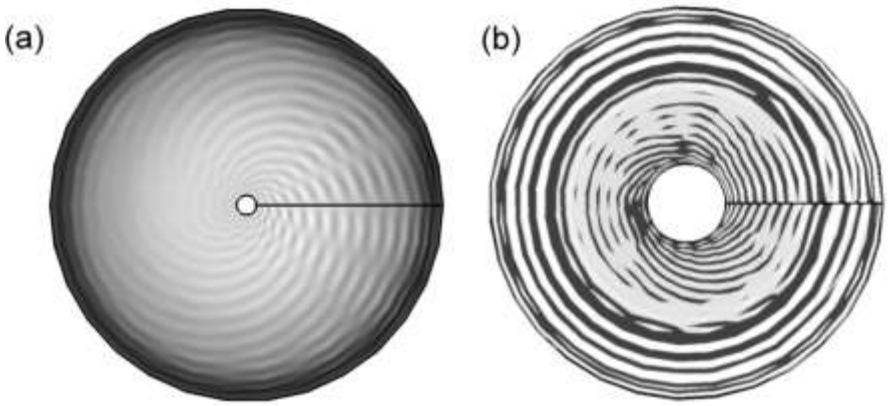

Figure 11. Iso-surfaces of the axial velocity component near the stator; Cases: (a) c3, and (b) c5.

5. Conclusions

A pseudospectral matrix-element method has been developed for simulating rotating flows in an annular cavity. To achieve this, the continuity and Navier-Stokes equations

have been solved in a three-dimensional cylindrical coordinate system using the modified compressibility method. Spectral grid convergence and and numerical stability tests were carried out, and the results demonstrate that the model provides reasonably accurate predictions of the rotating flow behavior, even when quite low numbers of collocation points are used. The numerical model is capable of reproducing the important features of laminar base flow and Type I and Type II instabilities of rotating flow in an annular cavity. Flow patterns, velocity time histories, and power spectra obtained for a parameter study in which the aspect ratio, Reynolds number, and curvature parameter are varied, are consistent with results with those from earlier numerical and experimental studies. Although no new flow physics has been discovered in the present study, it can be concluded that the PSME method offers considerable promise as a numerical technique for simulating rotating flows in annular rotor-stator cavities, particularly over a much broader range of parameters using higher resolution meshes.

Acknowledgments – The authors are grateful to the National Science Council of Taiwan for its generous financial support (NSC 99-2221-E-011-041). Also, the second author would like to express his gratitude for a Taiwan Scholarship from the National Science Council of Taiwan.

References

1. Batchelor, G. K., 1951. Note on a class of solutions of the Navier-Stokes equations representing steady rotationally-symmetric flow. Quarterly Journal of Mechanics and Applied Mathematics, 4(1): 29-41.

2. Boyd, J.P. and Yu, F., 2011. Comparing seven spectral methods for interpolation and for solving the Poisson equation in a disk: Zernike polynomials, Logan–Shepp ridge polynomials, Chebyshev–Fourier Series, cylindrical Robert functions, Bessel–Fourier expansions, square-to-disk conformal mapping and radial basis functions. Journal of Computational Physics, 230(4): 1408–1438.
3. Bödewadt, U.T., 1940. Die Drehströmung über festem Grunde. Zeitschrift für Angewandte Mathematik und Mechanik, 20(5): 241-253.
4. Canuto, C., Yousuff, H.M., Quarteroni, A. and Zang, T.A., 1988. Spectral methods in fluid dynamics. Springer-Verlag, Berlin-Heidelberg.
5. Chern, M.J. and Borthwick, A.G.L. and Eatock Taylor, R., 2001. Simulation of non-linear free surface motions in a cylindrical domain using a Chebyshev Fourier spectral collocation method. Int. Journal of Numerical Mathematics in Fluids, 36(4): 465–496.
6. Chern, M. J. and Borthwick, A.G.L. and Eatock Taylor, R., 2005. Pseudospectral element model for free surface viscous flows. International Journal of Numerical Methods for Heat & Fluid Flow, 15(6): 517 – 554.
7. Chern, M.J. and Vaziri, N. and Syamsuri, S. and Borthwick, A.G.L., 2011. Pseudospectral solution for three-dimensional non-linear sloshing in shallow water rectangular tank. Computer Methods in Applied Mechanics and Engineering (In press).
8. Chorin, A.J., 1968. Numerical solution of the Navier-Stokes equations. Mathematics of Computation, 22: 745-762.

9. Cortes, A.B. and Miller, J.D., 1994. Solution of the Navier-Stokes equations by the spectral-difference method. Numerical Methods for Partial Differential Equations, 10(3): 345-368.
10. Dijkstra, D. and van Heijst, G.J.F. 1983. The flow between two finite rotating disks enclosed by a cylinder. Journal of Fluid Mechanics, 128, 123-154.
11. Faller, A.J., 1991. Instability and transition of disturbed flow over a rotating disk. Journal of Fluid Mechanics, 230: 245-269.
12. Gauthier, G., Gondret, P. and Rabaud, M., 1999. Axisymmetric propagating vortices in the flow between a rotating and a stationary disk enclosed by a cylinder. Journal of Fluid Mechanics, 386: 105–126.
13. Hussaini, M.Y. and Zang, T.A., 1987. Spectral methods in fluid dynamics. Annual Review of Fluid Mechanics, 19: 339–367.
14. Itoh, M., 1991. On the instability of flow between coaxial rotating disks. Boundary Layer Stability and Transition to Turbulence, ASME FED, 114: 83-89.
15. Jennings, A. and McKeown, J.J., 1992. Matrix computation for engineers and scientists. John Wiley & Sons, Chichester.
16. Von Kármán, T., 1921. Über laminare und turbulente Reibung. Zeitschrift für Angewandte Mathematik und Mechanik, 1(4): 233-252.
17. Ku, H.C. and Hatziavramidis, D., 1985. Solutions of the 2-dimensional Navier-Stokes equations by Chebyshev expansion methods. Computers & Fluids, 13(1): 99–113.

18. Ku, H.C. and Hirsh, R.S. and Taylor, T.D., 1987. A pseudospectral method for solution of the three-dimensional incompressible Navier-Stokes equations. Journal of Computational Physics, 70(2): 439-462.
19. Lance, G.N. and Rogers, M.H., 1962. The axially symmetric flow of a viscous fluid between two infinite rotating disks. Proceedings of the Royal Society A, 266(1324): 109-121.
20. Launder, E. and Poncet, S. and Serre, E., 2010. Laminar, transitional and turbulent flows in rotor-stator cavities. Annual Review of Fluid Mechanics, 42: 229-248.
21. Lilly, D.K., 1966. On the instability of Ekman boundary layer. Journal of Atmospheric Sciences, 23(5): 481-494.
22. Maubert, P., Schiestel, R., Elena, L., Randriamampianina, A., Chaouche, A. M., Crespo del Arco, E. and Bontoux, P., 1993. Study of flow structure in rotating cavities: numerical predictions of laminar and turbulent, steady and unsteady flows. AGARD Heat Cooling and Mass Transfer in Gas Turbines, 23, 1-23.
23. Moisy, F., Doaré, O., Pasutto, T., Daube, O. and Rabaud, M., 2004. Experimental and numerical study of the shear layer instability between two counter-rotating disks. Journal of Fluid Mechanics, 504: 175–202.
24. Nore, C. and Tuskerman, L.S. and Daube, O. and Xin, S., 2003. The 1:2 mode interaction in exactly counter-rotating von Kármán swirling flow. Journal of Fluid Mechanics, 477: 51-88.

25. Owen, J.M. and Rogers, R.H., 1989. Flow and heat transfer in rotating-disc systems, Vol. 1: Rotor-Stator Systems. Research Studies Press, Taunton (John Wiley & Sons, New York).

26. Pearson C.E., 1965. Numerical solutions for the time-dependent viscous flow between two rotating coaxial disks. Journal of Fluid Mechanics, 21: 623–633.

27. Poncet, S., Serre, E. and Le Gal, P., 2009. Revisiting the two first instabilities of the flow in an annular rotor-stator cavity. Physics of Fluids, 21(6): 064106-064106-8.

28. Press, W.H. and Flannery, B.P. and Teukolsky, S.A. and Vetterling, W.T., 1986. Numerical Recipes. Cambridge University Press, Cambridge.

29. San'kov, P.I. and Smirnov, E.M., 1991. Stability of viscous flow between rotating and stationary disks. Fluid Dynamics, 26(6): 857-864.

30. Savas, Ö., 1987. Stability of Bödewadt flow. Journal of Fluid Mechanics, 183: 77-94.

31. Schouveiler, L., Le Gal, P., Chauve, M.P. and Takeda Y., 1999. Spiral and circular waves in the flow between a rotating and a stationary disk. Experiments in Fluids, 26(3): 179-187.

32. Schouveiler, L., Le Gal, P. and Chauve. M.P., 2001. Instabilities of the flow between a rotating and a stationary disk. Journal of Fluid Mechanics, 443, 329–350.

33. Serre, E., Crespo del Arco, E. and Bontoux, P., 2001. Annular and spiral patterns between rotating and stationary discs. Journal of Fluid Mechanics, 434, 65–100.

34. Serre, E. and Pulicani, J.-P., 2001. A 3D pseudospectral method for convection in a rotating cylinder. Computers and Fluids, 30(4): 491-519.

35. Serre, E. and Tuliszka-Sznitko, E. and Bontoux, P., 2004. Coupled numerical and theoretical study of the flow transition between a rotating and a stationary disk. Physics of Fluids, 16(3): 688–706.

36. Sirivat, A., 1991. Stability experiment of flow between a stationary and a rotating disk. Physics of Fluids A, 3, 2664-2671.

37. Stewartson, K., 1953. On the flow between two rotating coaxial discs. Proceedings of the Cambridge Philosophical Society, 49: 333-341.

38. Vaziri, N., Chern, M.J. and Borthwick, A.G.L., 2011. Pseudospectral σ-transformation model of solitary waves in a tank with uneven bed. Computers and Fluids, 49(1): 197-202.

39. Zandbergen, P.J. and Dijkstra, D., 1987. Von Kármán swirling flows. Annual Review of Fluid Mechanics, 19, 465-491.